In vivo long-term voltage imaging by genetically encoded voltage indicator reveals spatiotemporal dynamics of spinal cord neuronal populations during development

Asuka Shiraishi[1], Ayane Hayashi[2], Narumi Fukuda[1], Mari Hishinuma[1], Hiroaki Miyazawa[1], Sachiko Tsuda[1§]

1 Division of Life Science, Graduate School of Science and Engineering, Saitama University, 255 Shimo-Okubo, Sakura-ku, Saitama City, Saitama 338-8570, Japan

2 Department of Regulatory Biology, Faculty of Science, Saitama University, 255 Shimo-Okubo, Sakura-ku, Saitama City, Saitama 338-8570, Japan

[§]Author for correspondence (stsuda@mail.saitama-u.ac.jp)

Abstract

A central question of brain development lies in how individual neurons emerge and organize communities to acquire various functions. Voltage imaging provides unique approaches to address this by enabling simultaneous, non-invasive, in vivo recording of voltage dynamics from a population of cells. Recently, genetically encoded voltage indicators (GEVIs) facilitate cell-type specific imaging of voltage dynamics. However, it has not been applied to brain development. Here, we applied ArcLight, a GEVI utilizing voltage-sensitive domain, to zebrafish and established experimental approaches for analyzing voltage and morphology during development, focusing on the spinal cord and cerebellum. We initially demonstrated that Arclight was widely distributed in the neural tissues. By voltage imaging, we successfully visualized the coordinated, spontaneous activity of spinal cord neurons in their early stage of development at a high spatiotemporal resolution, at subcellular and population levels. Hyperpolarization and subthreshold signals were also detected. Finally, long-term voltage imaging during development revealed the process of changes in voltage dynamics in neuron populations, which were accompanied by axonal outgrowth. Voltage imaging could greatly contribute to our understanding of the functional organization of the nervous system during development.

Introduction

The nervous system consists of a large number of neurons that perform various functions. During development, these neurons are generated and communicate with each other to form functional networks. For a deeper understanding of brain function and development, it is essential to understand how the brain is formed and organized. However, such attempts are often hindered by the vast number of neurons. Optical methods provide a powerful approach to solving these difficulties because light facilitates non-invasive access to many neurons, which is difficult with electrophysiological techniques.

Voltage imaging enables fast, direct, and simultaneous detection of membrane potentials in a population of neurons, providing an excellent system for circuit analysis [1-3]. Its high speed and directness allow the detection of action potentials, hyperpolarization, and subthreshold responses, which are difficult to examine using calcium imaging, partly because of the slow kinetics of the indicators and the dynamics of calcium [4, 5]. Voltage imaging began with activity recording using voltage-sensitive dyes (VSDs) [6]. Subsequently, various types of VSDs have been developed to improve the brightness, signal-to-noise ratio, and wider variations in color, expanding our understanding of network dynamics and development in various brain regions [7-9]. In recent years, the development of genetically encoded voltage indicators (GEVIs) has progressed rapidly, resulting in cell-type-specific voltage imaging, which is difficult to achieve with VSDs. This yielded GEVIs with faster kinetics and brighter fluorescence, overcoming prior weaknesses in the speed and signal-to-noise ratio [10-12]. There are several types of GEVIs, based on their structures. One is a mosaic protein that uses the voltage-sensitive domain of voltage-sensitive phosphatases [13-16]. Another class of GEVIs uses the voltage sensitivity of microbial rhodopsins [17-20]. These GEVIs have been applied to the study of brain function for various brain regions [21-25]. However, in most studies, GEVI voltage imaging was used to undermine the function of neural circuits, and very few attempts have been made to understand brain development.

Here, to examine the dynamics of neuronal populations and their development,

we applied ArcLight to zebrafish, and established a series of recording approaches to expand the power of voltage imaging in developmental biology. Zebrafish is an optimal model system for developmental biology and neuroscience. The transparent and relatively small brain of zebrafish, together with various transgenic lines, provides an excellent system for analyzing the functional organization of the brain in various behavioral modalities by the whole-brain recordings [26, 27]. Several GEVIs have been successfully used for voltage imaging of the zebrafish brain, mainly to analyze the circuit functions [19, 20, 23, 24, 28]. In this study, we focus on the spinal cord and cerebellum, which are suitable for studying neural circuit development because of their rapid development, ease of observation, and accumulated information on circuit organization [29, 30].

The spinal cord contains neural circuits that play fundamental roles in locomotion. These circuits drive coordinated movements of the left and right sides of the body by a central pattern generator, which is a fundamental element of locomotion [31]. At an early stage of development, this coordinated activity emerges as the spontaneous firing of spinal cord neurons, which is considered important for circuit formation [32]. Although electrophysiological and optical studies have elucidated the firing dynamics of these neurons, the mechanisms by which this coordinated activity emerges remain to be understood [33-35]. This transient activity, known as fetal movement in mammals, has been observed as coiling movements during early development in zebrafish. In the spinal cord, this process leads to periodic bursts of alternating populations of neurons on the left and right sides [36, 37]. Previous studies have shown that such activity patterns emerge from uncorrelated activities within a few hours of early development [34, 37-39]. However, the mechanisms by which individual neurons emerge and constitute network function remain unclear. This is partly because previous studies have utilized either electrophysiology or calcium imaging, creating a large gap between precise information about the synaptic profiles of individual neurons and the population information obtained by calcium imaging. To solve this issue, we need to obtain voltage information from a population of neurons during the

course of circuit formation.

Cumulative information has been obtained about cerebellar circuits, which play pivotal roles in motor coordination, learning, and cognition, and are evolutionally highly conserved [29, 40]. Inhibition and high-frequency activity are prominent in the cerebellum and contribute to various adaptive properties of the cerebellum, including long-term depression, complex and simple spiking of Purkinje cells, modularity of the cerebellar circuitry, and activity-dependent pruning during development [41-45]. While VSD imaging has long been used to uncover cerebellar circuit dynamics, GEVI in the cerebellum, especially in its developmental process, is still limited [23, 42, 46].

Materials and Methods

Fish lines

Wild-type zebrafish (Danio rerio) with an RW genetic background or nacre line were used. Tg(elavl3:GAL4-VP16), Tg(hspGFFDMC28C;UAS:RFP), Tg(gSA2AzGFF152B;UAS:RFP), and Tg(UAS:lynRFP) fish lines have been described previously and obtained from the National BioResource Project [23, 47, 48]. The Tg lines were crossed with the nacre line [49]. All procedures were performed in accordance with a protocol approved by the Saitama University Committee on Animal Research.

DNA Construction and establishment of the ArcLight transgenic line

To generate the pTol2-UAS-ArcLight plasmid, ArcLight-A242 sequences were excited from the pCS2+/ArcLight-A242 plasmid (Addgene) and inserted into pTol2-UAS-MCSF-polyA, in which a UAS and polyA sequence was integrated into the pTol2-MCS plasmid [50]. pTol2-Aldoca-ArcLight-Q239-polyA construct was generated using a Purkinje cell-specific promoter, aldorace C, and the ArcLight-Q239 sequence. The ArcLight-Q239 and aldorace sequences were extracted from pCS2+/ArcLight-Q239 and aldoca-5k-pGEM-T_easy, respectively, and inserted into pTol2-UAS-MCSF-polyA pDNA. To establish pTol2-UAS-ArcLight

134 line, Tol2 plasmid DNA and transposase messenger RNA (mRNA) were co-
135 injected into one-cell-stage embryos. Genotyping was performed using the
136 primers ArcLight-A242 (5′-TCGACGGTATCGATAAGCTTGC-3′,5′-
137 CACCTCCCCCTGAACCTGAAACATA-3′).
138
139 **Transient expression of ArcLight in the cerebellum and spinal cord**
140 For the spinal cord, 25-ng/μl Tol2-UAS-ArcLight-A242-polyA plasmid DNA was
141 co-injected with 25-ng/μl *Tol2 transposase* mRNA into one-cell-stage embryos of
142 Tg(elavl3:GAL4-VP16) embryos, which express Gal4 in neurons [51] After the
143 injection, the embryos were incubated at 23°C and then transferred to 28°C by
144 18 hour post fertilization (hpf). ArcLight-positive embryos were screened at the
145 19-20 somite stage, followed by voltage imaging of the spinal cord at 20 to 24 hpf.
146 For the cerebellum, 5-40 ng/μl Tol2-Aldoca-ArcLight-Q239-polyA plasmid DNA
147 was co-injected with 25 ng/μl *Tol2 transposase* mRNA into one-cell-stage nacre
148 embryos. ArcLight-positive embryos were screened at 4 to 5 days post
149 fertilization (dpf), followed by voltage imaging at 5 to 6 dpf.
150
151 **Confocal imaging**
152 Zebrafish embryos were paralyzed in 0.02% tricaine and mounted on 2% low
153 melting-point agarose (Sigma-Aldrich). Optical sectioning was performed using
154 an Olympus FV1000 or a Nikon A1R (detector: A1-DU4) confocal microscope.
155 ImageJ, NIS-Elements (Nikon), and Imaris (Bitplane) software were used to
156 perform the image analysis.
157
158 **Voltage imaging of the spinal cord**
159 Embryos from 16 to 23 hpf were paralyzed with tubocurarine (0.5 mM, Sigma-
160 Aldrich), with their tail tips cut for better penetration of tubocurarine [37, 52]. Then,
161 embryos were mounted on 1.8% low melting-point agarose containing 0.1-0.2
162 mM tubocurarine. After embedding the embryos onto 1% agarose, an
163 extracellular solution (134 mM NaCl, 2.9 mM KCl, 2.1 mM $CaCl_2$, 1.2 mM $MgCl_2$,
164 10 mM HEPES, and 10 mM glucose, adjusted to pH 7.8 with NaOH) containing

150 mM tubocurarine was added. The agarose around the tail was removed using a surgical blade to allow efficient transfer of the drug solution. For high-speed voltage imaging, a fluorescence microscope (FN-1, Nikon) equipped with a CMOS camera (ORCA-Flash4.0, Hamamatsu Photonics) was used with a 40×/0.8 NA water-immersion lens. Fluorescence images were acquired using NIS-Elements (Nikon) software at approximately 16-200 Hz. High-speed confocal scanning was performed using a confocal microscope (Nikon A1R) with a 25×/1.0 NA water-immersion lens. For drug treatment, tetrodotoxin (1 μM, TOCRIS) was added to the extracellular solution using a peristatic pump (World Precision Instruments). A thermo plate was used to keep the recording chamber at 28°C (Tokai hit).

Voltage imaging of the cerebellum

Embryos from 5 to 9 dpf were paralyzed with 0.02% tricaine and transferred to an extracellular solution. Next, embryos were mounted on 2% low melting-point agarose. For imaging, a fluorescence microscope (FN-1, Nikon) equipped with a CMOS camera (ORCA-Flash4.0, Hamamatsu Photonics) was used with a 40×/0.8 NA water-immersion lens. Fluorescent images were acquired using NIS-Elements or HCImage (Hamamatsu Photonics) at approximately 50–200 Hz.

Image analysis

Images were analyzed using the NIS-Elements (Nikon), Fiji, and OriginPro (Lightstone) programs as described previously [52]. To extract changes in fluorescence intensity, regions of interest (ROIs) were manually set using NIS-element software (Nikon). Normalized changes in fluorescence intensity in the target regions (ROIs) were quantitatively analyzed by calculating dF/F in the ROIs ($dF/F0=[F(t)–F0]/F0$, where $F(t)$ and $F0$ are the fluorescence intensities at a certain time point and initial time points, respectively). If the larvae/embryos moved during the voltage imaging, the images were aligned using a Fiji program (TurboReg plugin). Denoising and bleach corrections were also applied to some data using OriginPro (Lightstone). Cross-correlation and hierarchical clustering

196 analyses were performed using OriginPro (Lightstone).
197
198
199 ## Results
200 ### Establishment of the ArcLight zebrafish line
201 To examine neuronal activity in the developing brain using voltage imaging, GEVI
202 ArcLight was used to establish transgenic zebrafish lines via the GAL4-UAS and
203 Tol2 transposon systems [27]. We generated a pTol2-UAS-ArcLight-A242-polyA
204 construct and established a transgenic line (Fig. 1a, b). To test whether ArcLight
205 was localized to the cellular membranes in Tg(UAS:ArcLight) fish, we observed
206 Tg(elavl3:GAL4-VP16;UAS:ArcLight;UAS:lyn-RFP) embryos, in which gal4 was
207 expressed in neurons, and the cellular membranes were labeled with Lyn-RFP.
208 At 1 dpf, ArcLight was widely observed in the neural tube and co-localized with
209 Lyn-RFP, indicating that ArcLight was properly distributed on the cellular
210 membrane in the neural tube (Fig. 1b, c). The distribution of ArcLight was also
211 examined in other brain regions, such as the cerebellum, using transgenic lines
212 expressing gal4 specifically in cerebellar neurons. Confocal imaging showed that
213 ArcLight was clearly expressed in granule cells and inferior olive neurons, which
214 are key components of cerebellar circuits [40] (Supplementary Figs. S1 and S2).
215 These results indicate that ArcLight is expressed in various neuron types in
216 developing zebrafish.
217
218 ### ArcLight could detect neural activity at the population and single-cell levels
219 Next, we performed high-speed imaging of the spinal cord of the Tg(elavl3:GAL4-
220 VP16;UAS:ArcLight) embryos. Spinal cord neurons show spontaneous firing at
221 the early stage of development, and this coordinated activity of the neuronal
222 populations begins at 17 hpf [34, 38, 39]. As shown in Figure 1, oscillatory
223 changes in ArcLight fluorescence intensity were detected in the ventral region of
224 somites 3–8 at 20 hpf at a frequency of 0.14±0.10 Hz (6 fish, Fig. 1d–g). Phases
225 of fluorescent changes differed between the left and right sides of the spinal cord
226 and occurred alternately, which is consistent with previous reports showing

227 periodic depolarization (PD) of spinal cord neurons (Warp et al., 2012). This
228 activity mostly disappeared after treatment with the sodium channel blocker
229 tetrodotoxin (TTX) (Fig. 1e-g; left side: control 0.14±0.10 Hz, TTX 0.01±0.02 Hz,
230 $p<0.05$, right side: control 0.14±0.10 Hz, TTX 0.01±0.02 Hz, $p<0.05$, Wilcoxon
231 signed-rank test, 6 fish). These data indicated that ArcLight can detect
232 spontaneous activity in developing zebrafish spinal cord neurons.
233 Next, we examined whether ArcLight enables the detection of neural activity at
234 the single-cell level. Figure 2 shows an example of the voltage imaging of the
235 spinal cord. Oscillatory activity was clearly detected in each neuron, and
236 differences in the size and pattern of activity between neighboring neurons were
237 visualized using ArcLight (Fig. 2a and b, 35 fish). In addition to large
238 depolarizations that closely resembled PD, slight membrane potential fluctuations
239 were also observed between the PDs (Fig. 2c). Their timing and patterns suggest
240 that they represent a subthreshold activity called a synaptic burst, which has been
241 reported in electrophysiological recordings (Saint-Amant & Drapeau, 2000).
242 Cross-correlation analysis revealed a strong positive correlation between the
243 ipsilateral neurons and a negative correlation between the contralateral neurons
244 (Fig. 2d). This result indicates that membrane potential changes are highly
245 synchronized between neurons on the ipsilateral side of the spinal cord at the
246 single-cell level, and that they alternate between the left and right sides.
247 Furthermore, the hierarchical clustering analysis suggested that populations of
248 neurons on the same side exhibited higher synchrony (Fig. 2e).
249
250 **High-spatiotemporal voltage imaging at the subcellular in the spinal cord**
251 Measuring membrane potential dynamics at the level of neuronal compartments
252 such as axons and dendrites is important for understanding information
253 processing in the brain [53]. To record the cell bodies and axons of the spinal cord
254 neurons, Tg(elavl3:GAL4-VP16;UAS:ArcLight) embryos between 20 and 23 hpf
255 were observed from their side (Fig. 3a). We focused on primary motor neurons
256 (PMNs), as they are easy to observe because of their distinguished morphology
257 (Fig. 3b). As shown in Figure 3, we successfully performed wide-field voltage

258 imaging and detected the membrane potential in the soma and proximo/distal
259 regions of the axons (13 fish). The soma and axons showed similar patterns of
260 depolarization, but the size of the membrane potential fluctuations tended to be
261 smaller in the axons than in the cell soma (Fig. 3b). Furthermore, recording at a
262 higher spatial resolution enabled illumination of filopodia dynamics and voltage
263 changes (Supplementary Fig. S3 and S4). Interestingly, we noticed that there
264 were areas within the axon where the amplitude of the membrane potential
265 dynamics was larger than that of the others (Supplementary Fig. S4).
266

267 **ArcLight mosaic labeling enables simultaneous single-cell observation of**
268 **morphology and neuronal activity**

269 Spinal cord circuits consist of many types of neurons whose position, morphology,
270 and physiological properties vary (Saint-Amant & Drapeau, 2001). To uncover the
271 circuit dynamics and development of neural circuits, it is essential to observe the
272 morphology and voltage dynamics of each component. For this purpose, the
273 aforementioned Tg(elavl3:GAL4-VP16;UAS:ArcLight) line has a weakness in that
274 a large number of neighboring neurons express ArcLight, making it challenging
275 to observe the morphology of individual cells. Therefore, we obtained both
276 recordings by expressing ArcLight in a mosaic manner.

277 By injecting UAS-ArcLight pDNA into Tg(elavl3:GAL4-VP16) fish, we obtained
278 embryos in which spinal cord neurons were sparsely labeled with ArcLight,
279 enabling clear detection of the dynamics of membrane potentials (Fig. 4a–c, 20
280 hpf, PMNs). We also succeeded in recording interneurons that were otherwise
281 difficult to identify (Fig. 4d and e). In addition to PD and synaptic burst-like activity,
282 some neurons exhibited hyperpolarization (Fig. 4e). In one hour, these neurons
283 changed their morphology; cell 2 extended a long axon; however, it did not show
284 depolarization (Supplementary Fig. S5).

285 We also attempted to perform voltage imaging of cerebellar Purkinje cells,
286 which play pivotal roles in the cerebellum; however, GEVI imaging of such cells
287 has not yet been reported. By injecting ArcLight DNA, which drives the expression
288 of ArcLight specifically in Purkinje cells, we obtained embryos with sparse

289 labeling of Purkinje cells (Supplementary Fig. S7a and b). Voltage imaging at 5
290 dpf revealed a change in fluorescence intensity, indicative of depolarization in
291 some Purkinje cells (Supplementary Fig. S7b–d). However, significant bleaching
292 makes long-term imaging difficult, and the membrane potential cannot be
293 recorded from multiple Purkinje cells. These results indicate that voltage imaging
294 using ArcLight enables measurement of the voltage dynamics of neurons at
295 various levels (population, single cell, and subcellular), providing a powerful
296 approach for analyzing neural circuits.
297
298 **Developmental changes in the membrane potentials of spinal neurons**
299 Next, we examined the developmental changes in voltage dynamics in neuron
300 populations. The periodic firing observed in the spinal cord of zebrafish embryos
301 corresponds to coiling behavior, which is homologous to fetal movements in
302 mammals and is suggested to be essential for circuit formation [32]. During
303 embryogenesis, this characteristic activity appears at approximately 17 hpf and
304 rapidly increases in frequency and amplitude until 20 hpf, followed by a gradual
305 decrease. However, the mechanism by which the cooperative activity of this
306 population of spinal neurons emerges and changes during development remains
307 unclear. To investigate voltage dynamics in populations of spinal cord neurons,
308 we performed voltage imaging of zebrafish embryos during this developmental
309 period.
310 As shown in Figure 5, voltage imaging was successfully performed for the first
311 time from the developing spinal cord continuously from 18 to 20 hpf (Fig. 5). At
312 18 hpf, a PMN located in the eight somite region had an axonal structure but
313 seldom exhibited burst activity. Instead, it often showed fluctuations in the voltage
314 signal (Fig. 5c, cell 1). This neuron gradually extended its axons, increasing the
315 number of burst firings at 18.5 hpf. By 19.5 hpf, the firing frequency quickly
316 reached 0.15 Hz. In the same embryo, we also obtained a recording from the
317 PMN located in 10 somite region (Fig. 5c, cell 2). At 18 hpf, cell 2 exhibited a short
318 protrusion near its soma, suggesting that it was about to extend its axons.

Interestingly, cell 2 appeared to have almost no activity at 18 hpf but started to show depolarization at 18.5 hpf. However, the pattern of membrane potential fluctuation was quite different from that of mature PMNs, with many cells showing a slow increase in depolarization. Additionally, small fluctuations in membrane potential were continuously detected, suggesting that they were subthreshold dynamics of membrane potentials in PMNs (Fig. 5c). By 19.5 hpf, cell2 extended the axon, while the frequency of bursts rapidly increased to reach 0.15 Hz. This tendency was also observed in the soma of cell 2 (Supplementary Fig. S6). A similar pattern of development was observed in other embryos (5 fish, 20 cells). These findings suggest that the coordinated activity in the spinal cord during the early stage develops through multiple steps: (1) no activity, (2) small membrane potential fluctuations and slow depolarization, and (3) oscillatory activity that coincides with axonal growth.

Next, we examined how the spontaneous activity in the spinal cord changes over time. Voltage imaging of a population of spinal cord neurons was performed from 20 to 23 hpf at 30-minute intervals (Fig. 6; Supplementary Fig. S8). The results showed that the regular and rapid population activity observed at 20 hpf decreased by 23 hpf, and there was also a change in the pattern, with the bursts becoming longer in duration (Fig. 6b). Furthermore, at 20 hpf, synchronized activity within ipsilateral neurons appeared regularly between the left and right sides; however, at 23 hpf, this regularity decreased, and several consecutive bursts of activity were observed on the same side of the spinal cord (Fig. 6b). Cross-correlation analysis revealed that at 20 hpf, both of ipsilateral and contralateral pairs of neurons showed a high degree of synchrony and periodicity in their activity (Fig. 6c). Again, they exhibited out-of-phase activity. In contrast, at 23 hpf, the periodicity in the ipsilateral and contralateral pairs, as well as the coordination between the left and right sides, seemed to be greatly reduced. In contrast, the contralateral pairs showed a reduction in synchrony, while the ipsilateral pairs maintained synchrony (Fig. 6c).

To confirm the stage differences in this activity pattern, the ratio of alternating activity between neurons located on the left and right sides of the spinal cord was

compared at 20–21 hpf and 23–24 hpf. At 20–21 hpf, almost all neurons showed alternating left-right activity, while at 23–24 hpf, this was significantly reduced to nearly 80% (Fig. 6d; 20–21 hpf: 98.9±1.10%; 23–24 hpf: 98.9±1.10%, 5 fish; 23–24 hpf: 79.8%±5.71%, 4 fish; $p<0.05$, Mann–Whitney U test). In contrast, all fish observed showed synchronous activity in the ipsilateral neurons at both developmental stages. These results suggest that in developing zebrafish spinal neurons, as the periodic activity acquired by 20 hpf gradually changes and disappears, left-right coordination is lost, but the correlation between ipsilateral neurons remains.

Discussion

GEVI voltage imaging is useful as it enables the recording of membrane potentials from many specific neuronal cell types noninvasively without using electrodes. However, it has not been applied to studying neurogenesis. In this study, we established experimental methods to enhance voltage imaging in the zebrafish cerebellum and spinal cord. These are important not only for analyzing neural circuits, but also for revealing developmental mechanisms.

Previously, electrophysiological recordings have been used to characterize membrane dynamics in the spinal cord. However, neurons were observed for a short period due to the invasive nature of the recordings. In addition, recordings were limited to single cells [54, 55]. Moreover, developmental analysis was performed using calcium imaging; however, in principle, it is impossible to record membrane potential dynamics using this method [37-39]. To the best of our knowledge, this is the first report of visualizing membrane potential dynamics in genetically defined neuronal populations during spinal cord development. Similarly, we believe that this is the first example of long-term GEVI-based imaging of neural circuit formation during development.

Voltage imaging of spinal cord neural circuits

In this study, we successfully established a transgenic zebrafish line expressing

ArcLight. Initially, we focused on the spinal cord: one of the earliest circuits to emerge during development, consisting of a relatively limited number of neurons [34]. Voltage imaging at 20 hpf showed that the spinal neuronal population exhibited regular, alternating left-right synchronous activity. The obtained patterns were clear, with similar patterns of voltage changes to those recorded by electrophysiology, but with higher resolution than those previously recorded using ASAP1 or calcium imaging (Miyazawa et al., 2018; Muto et al., 2011; Wan et al., 2019; Warp et al., 2012). This is probably because ArcLight has faster kinetics than the calcium sensor, and a higher signal-to-noise ratio than ASAP1[12, 56]. Previously, electrophysiological studies showed that most of the spinal cord neurons at the stage exhibit periodic bursts of activity called Periodic depolarization (PD) that drives tail-coiling behaviors (equivalent to human fetal movements). Similar patterns of burst firing, TTX dependence, suggesting that Na channels are important, and similar firing frequency all support the notion that the observed depolarization represents PD.

In addition to these suprathreshold activities, subthreshold activities, such as SB and hyperpolarization, were also detected by ArcLight. SB, which cannot be recorded using Ca imaging because it does not involve firing and is a small signal change, was captured by optical recording for the first time in this study. In the early developmental spinal cord, the contribution of chemical synapses is limited; many neurons have been shown to be connected by gap junctions [54]. ArcLight imaging might be able to visualize spatial information on electrical as well as chemical coupling, which is useful for circuit analysis. While further analysis is needed, including simultaneous electrophysiological recordings, this is the first non-invasive imaging of voltage dynamics in a spinal cord neurons population at their early stage of development.

High-resolution voltage imaging

Compartment-level analysis is important because neuronal function is regulated at the compartmental level, such as for dendritic computation and axonal compartments. ArcLight allowed recording separately from the cell body and axon

compartments of PMNs. Whilst most axons exhibited more activity proximally than distally, for some neurons, we also detected larger activity in the distal area. This may be due in part to the non-uniform distribution of sodium channels.

In addition, filopodia and lamellipodia were labeled by ArcLight, with filopodia also showing voltage dynamics. Further research is needed to understand the role of voltage changes in filopodia; for instance, in synapse formation and plasticity. Further extension of this technique to ratiometry voltage analysis is desirable for accurate recording [57]. The ability to simultaneously and noninvasively observe cell morphology and activity allows for a deeper understanding of network dynamics and their formation.

Emergence and changes in spinal cord networks during development

Long-term voltage imaging in the spinal cord showed that regular cooperative activity arises in parallel with axon outgrowth. For instance, PMNs were found to mature through multiple steps: (1) no firing, (2) small depolarization (initiation of axon outgrowth), (3) irregular cooperative activity, and (4) cooperative activity. This process proceeds in the same order in neurons distributed along the roster-caudal axis. Although it is known that spinal cord neurons without axonal outgrowth do not fire, this is the first time that stage-dependent changes have been demonstrated for the same population [54].

Notably, PMNs exhibited small fluctuations in membrane potentials before starting regular depolarization. Ion channels and gap junctions are key in driving membrane potential in early-stage spinal cord neurons [34], where the contribution of chemical synapses is limited, and many neurons are connected by gap junctions. Further research is needed to determine whether the observed small depolarization reflects, to some extent, spikelets. This could suggest that small fluctuation may be due to neuronal electrical coupling, as electrical synapses are a powerful trigger of synchronous activity [41, 58, 59]. Furthermore, evidence is still sparse on important questions; whether pattern generators exist, where they are located, and how they facilitate network activity [39]. Our approach with in vivo voltage imaging could provide further information.

444

445 **Voltage imaging in the cerebellum**

446 In the cerebellum, cumulative information on circuit dynamics was collected by
447 voltage-sensitive dye imaging [60-62]. To further understand circuit dynamics,
448 optical recording of membrane potentials in a cell-type-specific manner is
449 desirable. However, no study has clearly described cell-type-specific voltage
450 imaging using GEVIs, despite several systems being available for neuron-type-
451 specific expression [48]. In this study, we obtained strong ArcLight expression in
452 cerebellar granule cells and inferior olive neurons in our transgenic fish. As for
453 Purkinje cells, a central neuron in the cerebellum, we obtained ArcLight positive
454 cells using transient expression with a new construct, since strong expression
455 was not observed in Tg fish. Using voltage imaging, spontaneous depolarization
456 was detected in Purkinje cells. We assumed that this depolarization represented
457 a complex spike (CS), one of the key firing patterns of Purkinje cells, since the
458 frequency was similar to that of CSs detected by cell-attached
459 electrophysiological recordings at the same developmental stage in zebrafish [63].
460 However, we could not detect simple spikes (SSs) in Purkinje cells; this is partly
461 because SSs exhibit smaller amplitude and higher frequencies, making them
462 more difficult to target with voltage imaging [64, 65]. To improve the signal-to-
463 noise ratio of the recordings, stronger drivers for increasing GEVI expression,
464 more sensitive sensors, and an improved illumination/recording system are
465 desirable [12, 19, 66]. Although further validation with electrophysiology is
466 required, this work will provide an important step forward in understanding
467 information processing and development in the cerebellum.

468 Regarding GEVI expression, we noticed considerable differences in intensity
469 between neuron types, similar to other GEVIs such as ASAP1 [23]. To expand
470 GEVI voltage imaging for the analysis of various neuron types, it is important to
471 examine this difference in expression efficiency and to solve this issue.

472

473 In conclusion, this is the first report of simultaneous and non-invasive
474 recordings of membrane potentials from neuronal populations during

development using a GEVI. This approach allowed us to cultivate dynamic changes in their spatiotemporal patterns of activity. Our findings demonstrate that this experimental system is an effective tool for elucidating the mechanisms underlying neural circuit formation during development. Simple neuronal circuits connected by gap junctions are one of the key regulators in animal behavior, as shown in crab circuits [67]. Based on the imaging system we established for zebrafish, we would be able to further understand how complex activity and behaviors emerge from small populations of neurons by combining cell-type-specific recordings with manipulations of neuronal activity through optical, electrophysiological, and genetic approaches. Furthermore, in recent years, bioelectric signaling has gradually been found to be important for various biological phenomena, including morphogenesis; GEVI will be optimal to further investigate this area [68, 69].

Acknowledgement

We thank Drs M. Hibi, K. Kawakami, S. Higashijima, H. Okamoto, H. Kakinuma, and R. Omo for providing fish lines and a constructs, and J. Nakai, M. Ohkura, K. Ando, K. Yamasu, L. Cohen, K. Yamasu, and Y. Bando for technical supports and helpful discussion. This work was supported in part by JSPS KAKENHI (Grants-in-Aid for Scientific Research), JST Tenure Track program at Saitama University (SUTT), Strategic Research Program for Brain Science from Ministry of Education, Culture, Sports, Science, and Technology of Japan (ASTEP), Kao Foundation grant, Asahi Glass Foundation, and Kato-bio Foundation.

Author Contributions

S.A. and S.T. conceived and designed the experiments. S.A, A.H., N.F., M.H., K.M., and S.T. performed the experiments. S.A., A.H., N.F., H.M, and S.T wrote the manuscript. All authors reviewed the manuscript.

Additional Information

Competing interests

The authors declare no competing interests.

Data Availability

All data generated or analyzed in this study are included in the manuscript and supporting files.

Reference

1. Cohen, L.B. and B.M. Salzberg, *Optical measurement of membrane potential.* Rev Physiol Biochem Pharmacol, 1978. **83**: p. 35-88.
2. Loew, L.M., et al., *Evidence for a charge-shift electrochromic mechanism in a probe of membrane potential.* Nature, 1979. **281**(5731): p. 497-9.
3. Djurisic, M., et al., *Optical monitoring of neural activity using voltage-sensitive dyes.* Methods Enzymol, 2003. **361**: p. 423-51.
4. Lin, M.Z. and M.J. Schnitzer, *Genetically encoded indicators of neuronal activity.* Nat Neurosci, 2016. **19**(9): p. 1142-53.
5. Homma, R., et al., *Wide-field and two-photon imaging of brain activity with voltage- and calcium-sensitive dyes.* Philos Trans R Soc Lond B Biol Sci, 2009. **364**(1529): p. 2453-67.
6. Ross, W.N., et al., *Changes in absorption, fluorescence, dichroism, and Birefringence in stained giant axons: : optical measurement of membrane potential.* J Membr Biol, 1977. **33**(1-2): p. 141-83.
7. Yan, P., et al., *Palette of fluorinated voltage-sensitive hemicyanine dyes.* Proc Natl Acad Sci U S A, 2012. **109**(50): p. 20443-8.
8. Wuskell, J.P., et al., *Synthesis, spectra, delivery and potentiometric responses of new styryl dyes with extended spectral ranges.* J Neurosci Methods, 2006. **151**(2): p. 200-15.
9. Momose-Sato, Y., T. Nakamori, and K. Sato, *Spontaneous depolarization wave in the mouse embryo: origin and large-scale propagation over the CNS identified with voltage-sensitive dye imaging.* Eur J Neurosci, 2012. **35**(8): p. 1230-41.
10. Storace, D., et al., *Toward Better Genetically Encoded Sensors of Membrane Potential.* Trends Neurosci, 2016. **39**(5): p. 277-289.
11. Kannan, M., G. Vasan, and V.A. Pieribone, *Optimizing Strategies for Developing Genetically Encoded Voltage Indicators.* Front Cell Neurosci, 2019. **13**: p. 53.
12. Bando, Y., et al., *Comparative Evaluation of Genetically Encoded Voltage Indicators.* Cell Rep, 2019. **26**(3): p. 802-813 e4.
13. Akemann, W., et al., *Imaging neural circuit dynamics with a voltage-sensitive fluorescent protein.* J Neurophysiol, 2012. **108**(8): p. 2323-37.
14. Jin, L., et al., *Single action potentials and subthreshold electrical events imaged in neurons with a fluorescent protein voltage probe.* Neuron, 2012. **75**(5): p. 779-85.
15. St-Pierre, F., et al., *High-fidelity optical reporting of neuronal electrical activity with*

550 *an ultrafast fluorescent voltage sensor.* Nat Neurosci, 2014. **17**(6): p. 884-9.
551 16. Tsutsui, H., et al., *Improving membrane voltage measurements using FRET with*
552 *new fluorescent proteins.* Nat Methods, 2008. **5**(8): p. 683-5.
553 17. Hochbaum, D.R., et al., *All-optical electrophysiology in mammalian neurons*
554 *using engineered microbial rhodopsins.* Nat Methods, 2014. **11**(8): p. 825-33.
555 18. Gong, Y., et al., *High-speed recording of neural spikes in awake mice and flies*
556 *with a fluorescent voltage sensor.* Science, 2015. **350**(6266): p. 1361-6.
557 19. Abdelfattah, A.S., et al., *Bright and photostable chemigenetic indicators for*
558 *extended in vivo voltage imaging.* Science, 2019. **365**(6454): p. 699-704.
559 20. Piatkevich, K.D., et al., *A robotic multidimensional directed evolution approach*
560 *applied to fluorescent voltage reporters.* Nat Chem Biol, 2018. **14**(4): p. 352-360.
561 21. Nakajima, R. and B.J. Baker, *Mapping of excitatory and inhibitory postsynaptic*
562 *potentials of neuronal populations in hippocampal slices using the GEVI, ArcLight.*
563 J Phys D Appl Phys, 2018. **51**(50).
564 22. Storace, D.A. and L.B. Cohen, *Measuring the olfactory bulb input-output*
565 *transformation reveals a contribution to the perception of odorant concentration*
566 *invariance.* Nat Commun, 2017. **8**(1): p. 81.
567 23. Miyazawa, H., et al., *Optical interrogation of neuronal circuitry in zebrafish using*
568 *genetically encoded voltage indicators.* Sci Rep, 2018. **8**(1): p. 6048.
569 24. Bohm, U.L., et al., *Voltage imaging identifies spinal circuits that modulate*
570 *locomotor adaptation in zebrafish.* Neuron, 2022. **110**(7): p. 1211-1222 e4.
571 25. Yang, H.H., et al., *Subcellular Imaging of Voltage and Calcium Signals Reveals*
572 *Neural Processing In Vivo.* Cell, 2016. **166**(1): p. 245-57.
573 26. Ahrens, M.B., et al., *Brain-wide neuronal dynamics during motor adaptation in*
574 *zebrafish.* Nature, 2012. **485**(7399): p. 471-7.
575 27. Asakawa, K., et al., *Genetic dissection of neural circuits by Tol2 transposon-*
576 *mediated Gal4 gene and enhancer trapping in zebrafish.* Proc Natl Acad Sci U S
577 A, 2008. **105**(4): p. 1255-60.
578 28. Yoshimatsu, T., et al., *Ancestral circuits for vertebrate color vision emerge at the*
579 *first retinal synapse.* Sci Adv, 2021. **7**(42): p. eabj6815.
580 29. Hashimoto, M. and M. Hibi, *Development and evolution of cerebellar neural*
581 *circuits.* Dev Growth Differ, 2012. **54**(3): p. 373-89.
582 30. McLean, D.L., et al., *A topographic map of recruitment in spinal cord.* Nature,
583 2007. **446**(7131): p. 71-5.
584 31. Grillner, S., *Neurobiological bases of rhythmic motor acts in vertebrates.* Science,
585 1985. **228**(4696): p. 143-9.

586 32. Menelaou, E., et al., *Embryonic motor activity and implications for regulating*
587 *motoneuron axonal pathfinding in zebrafish.* Eur J Neurosci, 2008. **28**(6): p. 1080-
588 96.
589 33. Fidelin, K. and C. Wyart, *Inhibition and motor control in the developing zebrafish*
590 *spinal cord.* Curr Opin Neurobiol, 2014. **26C**: p. 103-109.
591 34. Saint-Amant, L., *Development of motor rhythms in zebrafish embryos.* Prog Brain
592 Res, 2010. **187**: p. 47-61.
593 35. O'Donovan, M.J., *The origin of spontaneous activity in developing networks of*
594 *the vertebrate nervous system.* Curr Opin Neurobiol, 1999. **9**(1): p. 94-104.
595 36. Saint-Amant, L. and P. Drapeau, *Motoneuron activity patterns related to the*
596 *earliest behavior of the zebrafish embryo.* J Neurosci, 2000. **20**(11): p. 3964-72.
597 37. Muto, A., et al., *Genetic visualization with an improved GCaMP calcium indicator*
598 *reveals spatiotemporal activation of the spinal motor neurons in zebrafish.* Proc
599 Natl Acad Sci U S A, 2011. **108**(13): p. 5425-30.
600 38. Warp, E., et al., *Emergence of patterned activity in the developing zebrafish*
601 *spinal cord.* Curr Biol, 2012. **22**(2): p. 93-102.
602 39. Wan, Y., et al., *Single-Cell Reconstruction of Emerging Population Activity in an*
603 *Entire Developing Circuit.* Cell, 2019. **179**(2): p. 355-372 e23.
604 40. Ito, M., *Cerebellar circuitry as a neuronal machine.* Prog Neurobiol, 2006. **78**(3-
605 5): p. 272-303.
606 41. Mann-Metzer, P. and Y. Yarom, *Electrotonic coupling interacts with intrinsic*
607 *properties to generate synchronized activity in cerebellar networks of inhibitory*
608 *interneurons.* J Neurosci, 1999. **19**(9): p. 3298-306.
609 42. Cohen, D. and Y. Yarom, *Patches of synchronized activity in the cerebellar cortex*
610 *evoked by mossy-fiber stimulation: questioning the role of parallel fibers.* Proc
611 Natl Acad Sci U S A, 1998. **95**(25): p. 15032-6.
612 43. Whittington, M.A., R.D. Traub, and J.G. Jefferys, *Synchronized oscillations in*
613 *interneuron networks driven by metabotropic glutamate receptor activation.*
614 Nature, 1995. **373**(6515): p. 612-5.
615 44. Ito, M., *Cerebellar long-term depression.* Trends Neurosci, 1996. **19**(1): p. 11-12.
616 45. Apps, R. and R. Hawkes, *Cerebellar cortical organization: a one-map hypothesis.*
617 Nat Rev Neurosci, 2009. **10**(9): p. 670-81.
618 46. Tsuda, S., et al., *Probing the function of neuronal populations: combining*
619 *micromirror-based optogenetic photostimulation with voltage-sensitive dye*
620 *imaging.* Neurosci Res, 2013. **75**(1): p. 76-81.
621 47. Kimura, Y., C. Satou, and S. Higashijima, *V2a and V2b neurons are generated*

by the final divisions of pair-producing progenitors in the zebrafish spinal cord. Development, 2008. **135**(18): p. 3001-5.

48. Takeuchi, M., et al., *Establishment of Gal4 transgenic zebrafish lines for analysis of development of cerebellar neural circuitry.* Dev Biol, 2015. **397**(1): p. 1-17.
49. Lister, J.A., et al., *nacre encodes a zebrafish microphthalmia-related protein that regulates neural-crest-derived pigment cell fate.* Development, 1999. **126**(17): p. 3757-67.
50. Nakayama, Y., et al., *Comprehensive analysis of target genes in zebrafish embryos reveals gbx2 involvement in neurogenesis.* Dev Biol, 2017. **430**(1): p. 237-248.
51. Kimura, Y., et al., *Hindbrain V2a neurons in the excitation of spinal locomotor circuits during zebrafish swimming.* Curr Biol, 2013. **23**(10): p. 843-9.
52. Hiyoshi, K., et al., *In vivo wide-field voltage imaging in zebrafish with voltage-sensitive dye and genetically encoded voltage indicator.* Dev Growth Differ, 2021. **63**(8): p. 417-428.
53. London, M. and M. Hausser, *Dendritic computation.* Annu Rev Neurosci, 2005. **28**: p. 503-32.
54. Saint-Amant, L. and P. Drapeau, *Synchronization of an embryonic network of identified spinal interneurons solely by electrical coupling.* Neuron, 2001. **31**(6): p. 1035-46.
55. Saint-Amant, L. and P. Drapeau, *Time course of the development of motor behaviors in the zebrafish embryo.* J Neurobiol, 1998. **37**(4): p. 622-32.
56. Storace, D.A., et al., *Monitoring brain activity with protein voltage and calcium sensors.* Sci Rep, 2015. **5**: p. 10212.
57. Kim, B.B., et al., *A red fluorescent protein with improved monomericity enables ratiometric voltage imaging with ASAP3.* Sci Rep, 2022. **12**(1): p. 3678.
58. Epsztein, J., et al., *Impact of spikelets on hippocampal CA1 pyramidal cell activity during spatial exploration.* Science, 2010. **327**(5964): p. 474-7.
59. de Solages, C., et al., *High-frequency organization and synchrony of activity in the purkinje cell layer of the cerebellum.* Neuron, 2008. **58**(5): p. 775-88.
60. Roome, C.J. and B. Kuhn, *Simultaneous dendritic voltage and calcium imaging and somatic recording from Purkinje neurons in awake mice.* Nat Commun, 2018. **9**(1): p. 3388.
61. Rokni, D., R. Llinas, and Y. Yarom, *Stars and stripes in the cerebellar cortex: a voltage sensitive dye study.* Front Syst Neurosci, 2007. **1**: p. 1.
62. Okumura, K., et al., *Optical measurement of neuronal activity in the developing*

cerebellum of zebrafish using voltage-sensitive dye imaging. Neuroreport, 2018. **29**(16): p. 1349-1354.

63. Hsieh, J.Y., et al., *Rapid development of Purkinje cell excitability, functional cerebellar circuit, and afferent sensory input to cerebellum in zebrafish.* Front Neural Circuits, 2014. **8**: p. 147.
64. Knogler, L.D., A.M. Kist, and R. Portugues, *Motor context dominates output from purkinje cell functional regions during reflexive visuomotor behaviours.* Elife, 2019. **8**.
65. Harmon, T.C., et al., *Distinct responses of Purkinje neurons and roles of simple spikes during associative motor learning in larval zebrafish.* Elife, 2017. **6**.
66. Namikawa, K., et al., *Modeling Neurodegenerative Spinocerebellar Ataxia Type 13 in Zebrafish Using a Purkinje Neuron Specific Tunable Coexpression System.* J Neurosci, 2019. **39**(20): p. 3948-3969.
67. Gutierrez, G.J., T. O'Leary, and E. Marder, *Multiple mechanisms switch an electrically coupled, synaptically inhibited neuron between competing rhythmic oscillators.* Neuron, 2013. **77**(5): p. 845-58.
68. Levin, M., *Bioelectric signaling: Reprogrammable circuits underlying embryogenesis, regeneration, and cancer.* Cell, 2021. **184**(8): p. 1971-1989.
69. Harris, M.P., *Bioelectric signaling as a unique regulator of development and regeneration.* Development, 2021. **148**(10).

680 **Figure Legends**

681

682 **Figure 1**

683 Transgenic zebrafish showing membrane-localized ArcLight and spontaneous
684 activity in the neural tube. (a) Schematic diagram of plasmid construct for ArcLight.
685 (b) Lateral views of ArcLight-expressing embryos at 1 dpf. ArcLight is distributed
686 widely in the neural tube of Tg(elavl3:GAL4-VP16;UAS:ArcLight) fish. (c) Dorsal
687 view of the neural tube of Tg(elavl3:GAL4-VP16;UAS:ArcLight;UAS:lyn-RFP)
688 embryos at 1 dpf. ArcLight (green) is co-localized with Lyn-RFP (red: cell
689 membranes) in the neural tube (arrowheads). Higher magnification images are
690 shown in the lower panel. (d-f) Spontaneous activity of spinal cord neurons is
691 detected by ArcLight imaging. (d) Dorsal view of the ventral spinal cord of Tg
692 (elavl3:GAL4-VP16;UAS:ArcLight-A242) fish at 20 hpf. The rostral side is to the
693 left, and the area between 3–8 somites is shown. A schematic diagram of the
694 imaging system is shown on the right. Changes in fluorescence of ArcLight
695 ($-\Delta F/F_0$) are indicated by the pseudocolor scale shown at right. White
696 arrowheads indicate the activated neurons. Regions of interest (ROIs) located
697 between 5–7 somites are indicated by red (right side) and blue (left side)
698 rectangular in (d). Fluorescence changes of ArcLight in the ROIs are shown in
699 the right. The time point of the image is indicated by a black arrowhead. (f-g) The
700 spontaneous activity in the spinal cord mostly disappeared by tetrodotoxin (TTX)
701 treatment (6 fish, *: $p < 0.05$). The imaged plane and ROIs are in the same positions
702 as in (d).

703

704 **Figure 2**

705 Monitoring of spontaneous activity of individual cells in the spinal cord by ArcLight
706 imaging. (a) A fluorescence image of the ventral spinal cord of Tg(elavl3:GAL4-
707 VP16;UAS:ArcLight) fish at 21 hpf. ROIs are located at the 18 cells (red: right
708 side, blue: left side). Higher magnification views are shown on the right. (b)
709 Changes in ArcLight signals fluorescence of ArcLight at the two time points
710 indicated in (c). (c) Activity patterns of the 18 cells are shown. A higher

711 magnification view of the ArcLight signal of cell 4 is shown at the bottom. (b). (d,
712 e) Hierarchal clustering analysis of the voltage dynamics in the 18 cells shows
713 the synchronous activity in the ipsilateral neuron pairs (d), and also several
714 groups with higher synchrony within them.
715
716 **Figure 3**
717 Voltage imaging of spinal cord neurons at a high spatiotemporal resolution at the
718 cellular compartment level by ArcLight. (a) Lateral view of the spinal cord of
719 Tg(elavl3:GAL4-VP16;UAS:ArcLight) fish at 20 hpf. (b) Changes in ArcLight
720 signal are observed at soma and axons in three different ROIs shown in (a).
721 Higher resolution observations are shown in Supplementary Fig. S3 and S4.
722
723 **Figure 4**
724 Single cell labeling of neurons by ArcLight enables simultaneous recording of
725 voltage and morphology. (a) Schematic diagram of the co-injection experiment.
726 (b) A stacked confocal image of the spinal cord region of the injected embryo at
727 20 hpf. The left side view is shown. Arrowheads and arrows indicate the soma
728 and axons of ArcLight positive cells, respectively. (c) Voltage dynamics of a
729 primary motor neuron are indicated by a yellow arrowhead in (b). ROIs at soma
730 and axons are shown in red and blue, respectively. (d, e) Voltage imaging of the
731 spinal cord interneurons. A higher magnification view is shown in e. ArcLight
732 signals from three cells are shown on the right. In addition to periodic
733 depolarization, hyperpolarization (white arrowheads) and subthreshold-like
734 signals (black arrowheads) are observed.
735
736 **Figure 5**
737 Long-term voltage imaging of the spinal cord shows the emergence of population
738 activity. (a) Left views of the spinal cord of ArcLight positive fish from 18 hpf to
739 19.5 hpf. (b) Enlarged views of (a). (c) Voltage dynamics obtained from the axons
740 of the two cells shown in (a). Arrowheads indicate small depolarization.
741

742 **Figure 6**

743 Changes in firing properties in spinal cord neuron populations. (a) Dorsal view of
744 ArcLight positive spinal cord at 20 hpf. (b) Voltage dynamics of each neuron are
745 shown at 20 and 23 hpf. The position of ROIs is indicated in (a). (c) Cross-
746 correlation analysis of ipsilateral and contralateral pairs of spinal cord neurons at
747 20 and 23 hpf. (d) Probability of altering activity at 20-21 hpf and 23-24 hpf.

748

749

750

751 **Supplementary Figure S1**

752 ArcLight (green) is distributed in cerebellar granule cells (red). Dorsal view of the
753 cerebellum of Tg(hspGFFDMC152C;UAS:RFP;UAS:ArcLight) fish observed at 6
754 dpf. Higher magnification views are shown in the lower panel.

755

756

757 **Supplementary Figure S2**

758 ArcLight is expressed in inferior olivary neurons. (a) Dorsal view of the inferior
759 olive (IO) of Tg(hspGFFDMC28C;UAS:RFP;UAS:ArcLight) fish at 8 dpf.
760 Arrowheads in the cerebellum (CE) indicate ArcLight signals (green) in the
761 climbing fibers. (b) (left) Schematic diagram of the co-injection experiment. (right)
762 Transient expression of ArcLight in a single IO neuron. Higher magnification
763 views are shown in the right panel.

764

765

766 **Supplementary Figure S3**

767 Confocal observation of ArcLight expression and voltage dynamics in the spinal
768 cord. (a) Lateral views of Tg(elavl3:GAL4-VP16;UAS:ArcLight) embryo at 1 dpf.
769 Higher magnification images shown in the right indicate filopodia and lamerioidia
770 of primary motor neurons (arrowheads). (b) Voltage imaging of cell1 in (a). ROIs
771 were set at the axonal region. ArcLight detected depolarization at axons (black
772 arrowheads). The gray area is the period when the embryos moved.

773
774
775 **Supplementary Figure S4**
776 Voltage imaging of a primary motor neuron at higher spatial resolution. (a) Left
777 views of the spinal cord at two different time points. Arrowheads indicate filopodia
778 (white, yellow). A yellow arrowhead indicates a filopodium that shows a prominent
779 extension. (b, c) An example of voltage dynamics detected at various positions in
780 the axon. ROI4-6 were set on a filopodium. ROI 7 was set in a region where no
781 clear structure was observed.
782
783
784 **Supplementary Figure S5**
785 Single-cell labeling by ArcLight shows the morphological changes of the spinal
786 cord neurons. Images taken at 21 hpf and 22 hpf are shown. An arrowhead
787 indicates a growth cone of the extending axon.
788
789
790 **Supplementary Figure S6**
791 ArcLight imaging in Purkinje cells. (a) (top) Schematic diagram ofpTo2-aldoca-
792 ArcLightQ239-polyA construct. (bottom) ArcLight is expressed in Purkinje cells in
793 the cerebellum (CE). Arrowheads and an arrow indicate Purkinje cell soma and
794 dendrite, respectively. A higher magnification view is shown on the right. (b-d)
795 ArcLight imaging exhibits depolarization in Purkinje cells. (b) ArcLight signal in
796 the recorded Purkinje cells. (c) Depolarization signals are observed by ArcLight
797 imaging (arrowheads). (d) Enlarged views of the traces are shown in (c).
798
799 **Supplementary Figure S7**
800 ArcLight imaging in Purkinje cells. (a) (top) Schematic diagram ofpTo2-aldoca-
801 ArcLightQ239-polyA construct. (bottom) ArcLight is expressed in Purkinje cells in
802 the cerebellum (CE). Arrowheads and an arrow indicate Purkinje cell soma and
803 dendrite, respectively. A higher magnification view is shown on the right. (b-d)

804 ArcLight imaging exhibits depolarization in Purkinje cells. (b) ArcLight signal in
805 the recorded Purkinje cells. (c) Depolarization signals are observed by ArcLight
806 imaging (arrowheads). (d) Enlarged views of the traces are shown in (c).
807
808
809 **Supplementary Figure S7**
810 Long-term voltage imaging shows the changes in the firing patterns of the spinal
811 cord neurons population. (a) ROIs position of cells 1-6. (b) Voltage dynamics of
812 6 cells are shown from 20 to 23 hpf. Cells on the right and left sides of the spinal
813 cord are shown in red and blue, respectively.
814
815
816 **Supplementary Movie1**
817 Spontaneous activity of individual cells in the spinal cord is observed by ArcLight.
818 Dorsal view of the ventral spinal cord of Tg(elavl3:GAL4-VP16;UAS:ArcLight) fish
819 at 21 hpf.
820
821
822 **Supplementary Movie2**
823 Monitoring of spontaneous activity of spinal cord neurons, including primary
824 motor neurons by ArcLight. Left view of the spinal cord of Tg(elavl3:GAL4-
825 VP16;UAS:ArcLight) fish at 20 hpf.
826
827
828 **Supplementary Movie3**
829 Single-cell labeling and voltage imaging of spinal cord neurons using ArcLight.
830 Left view of the spinal cord of Tg(elavl3:GAL4-VP16) embryo at 21 hpf. A high-
831 resolution image is shown in Supplementary Figure S5.
832
833
834 **Supplementary Movie4**

Voltage dynamics of an axonal region of a primary motor neuron at a high spatial resolution. Left view of the spinal cord Tg(elavl3:GAL4-VP16;UAS:ArcLight) fish at 18.5 hpf.

Figure 1

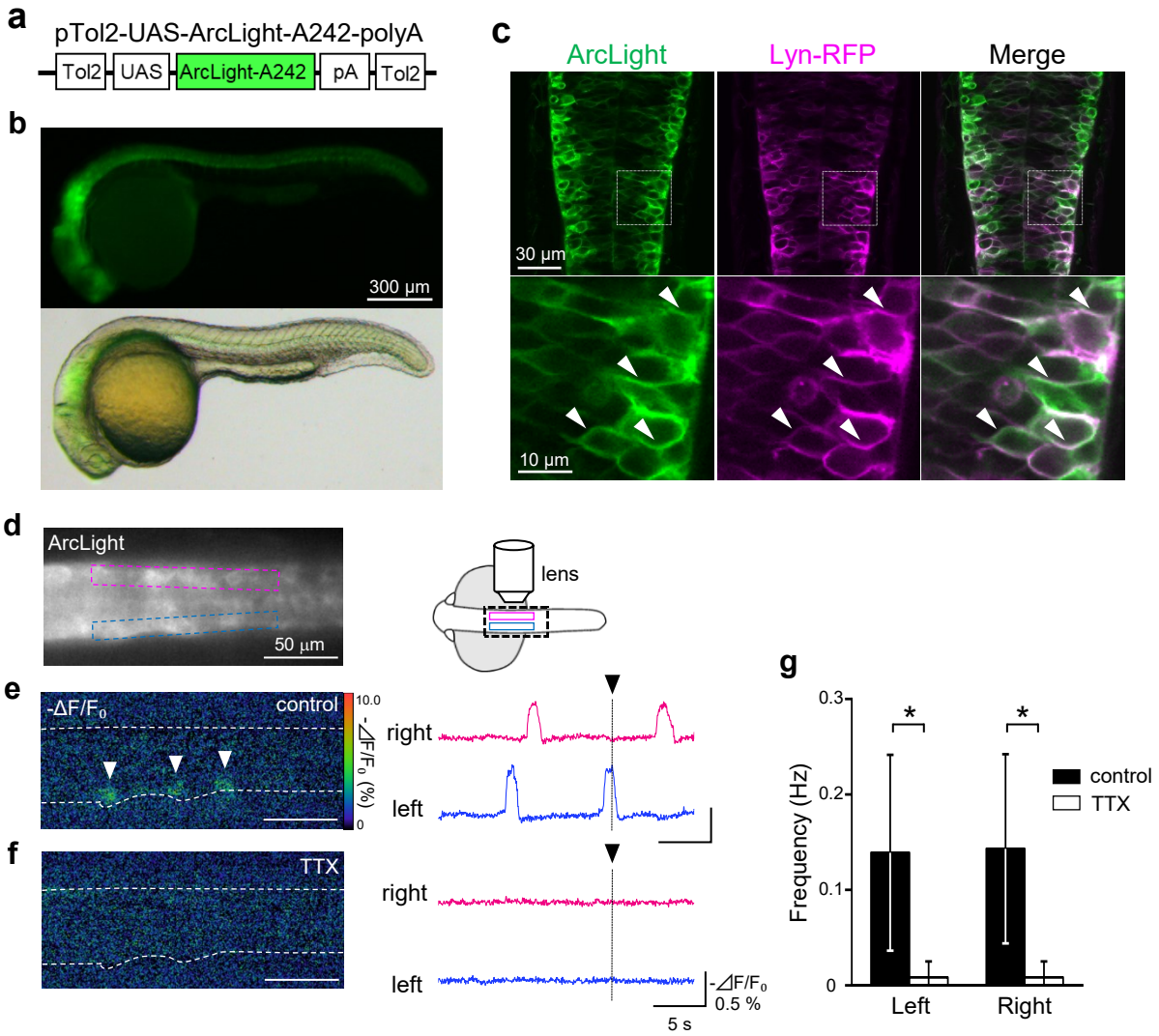
a
pTol2-UAS-ArcLight-A242-polyA
Tol2
UAS
ArcLight-A242
pA
Tol2
b
300 μm
c
ArcLight
Lyn-RFP
Merge
30 μm
10 μm
d
ArcLight
50 μm
lens
e
-ΔF/F0
control
10.0
-ΔF/F0 (%)
0
f
TTX
right
left
right
left
-ΔF/F0
0.5 %
5 s
g
0.3
0.2
0.1
0
Frequency (Hz)
*
*
control
TTX
Left
Right

Figure 2

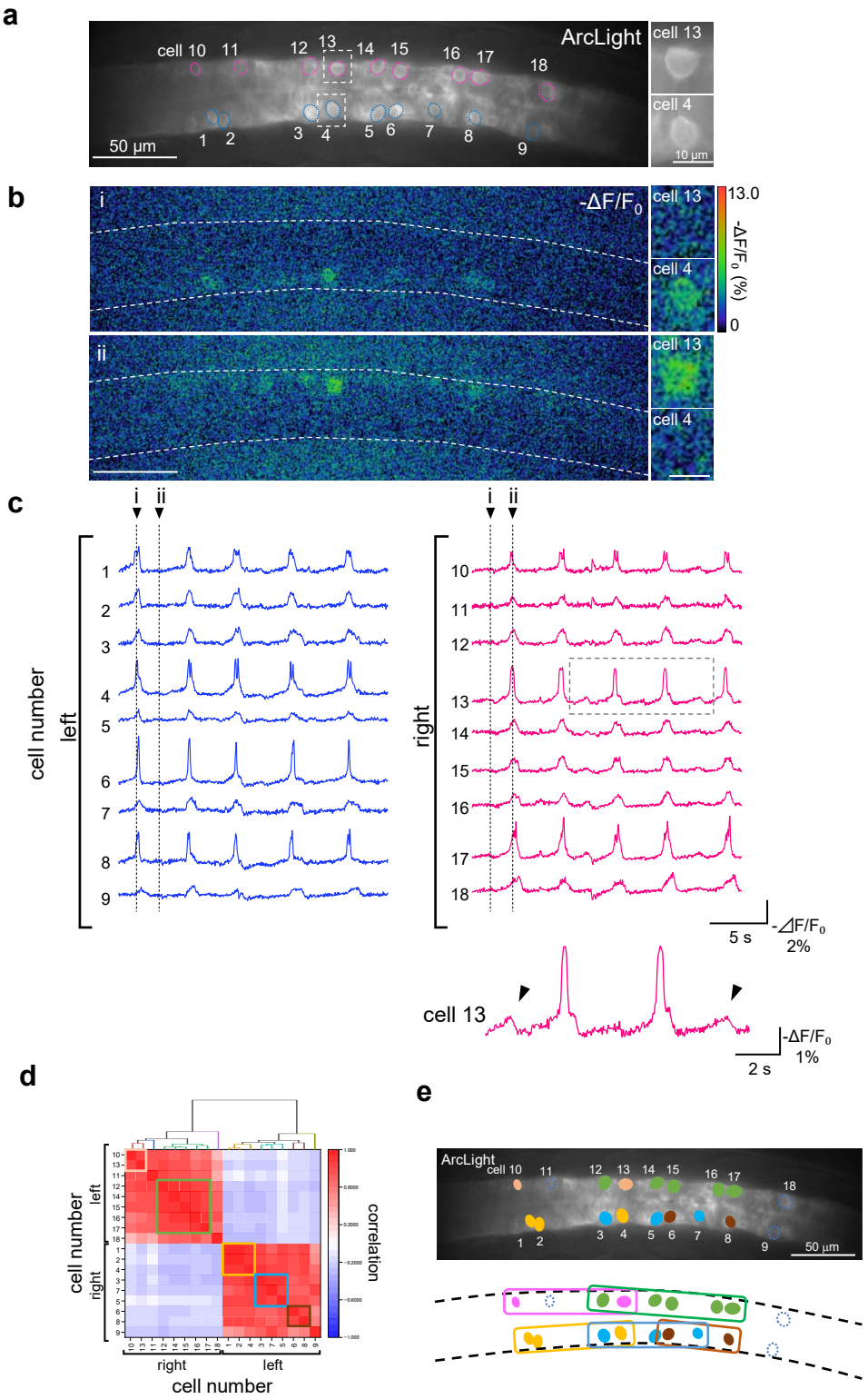
a
ArcLight
cell 10
11
12
13
14
15
16
17
18
1
2
3
4
5
6
7
8
9
50 µm
cell 13
cell 4
10 µm
b
i
ii
-ΔF/F0
cell 13
cell 4
13.0
-ΔF/F0 (%)
0
c
cell number
left
right
5 s
-ΔF/F0
2%
cell 13
2 s
1%
d
cell number
left
right
correlation
e
ArcLight
50 µm

Figure 3

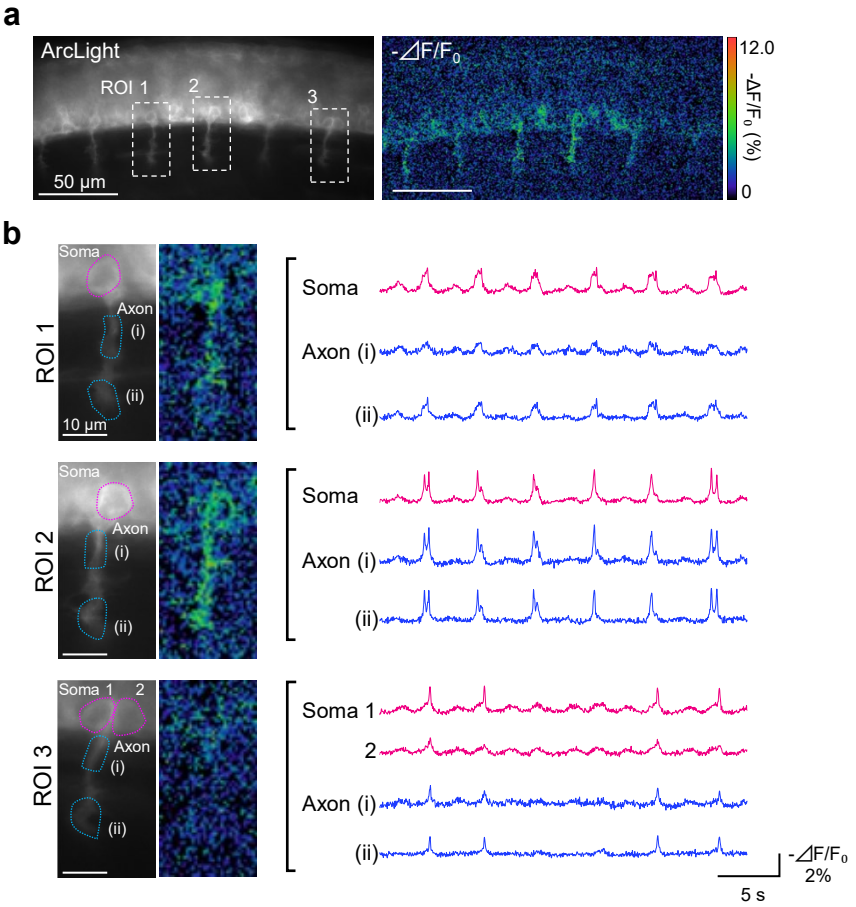
a
ArcLight
ROI 1
2
3
50 μm
-⊿F/F0
12.0
-ΔF/F0 (%)
0
b
ROI 1
Soma
Axon
(i)
(ii)
10 μm
Soma
Axon (i)
(ii)
ROI 2
Soma
Axon
(i)
(ii)
Soma
Axon (i)
(ii)
ROI 3
Soma 1
2
Axon
(i)
(ii)
Soma 1
2
Axon (i)
(ii)
-⊿F/F0
2%
5 s

Figure 4

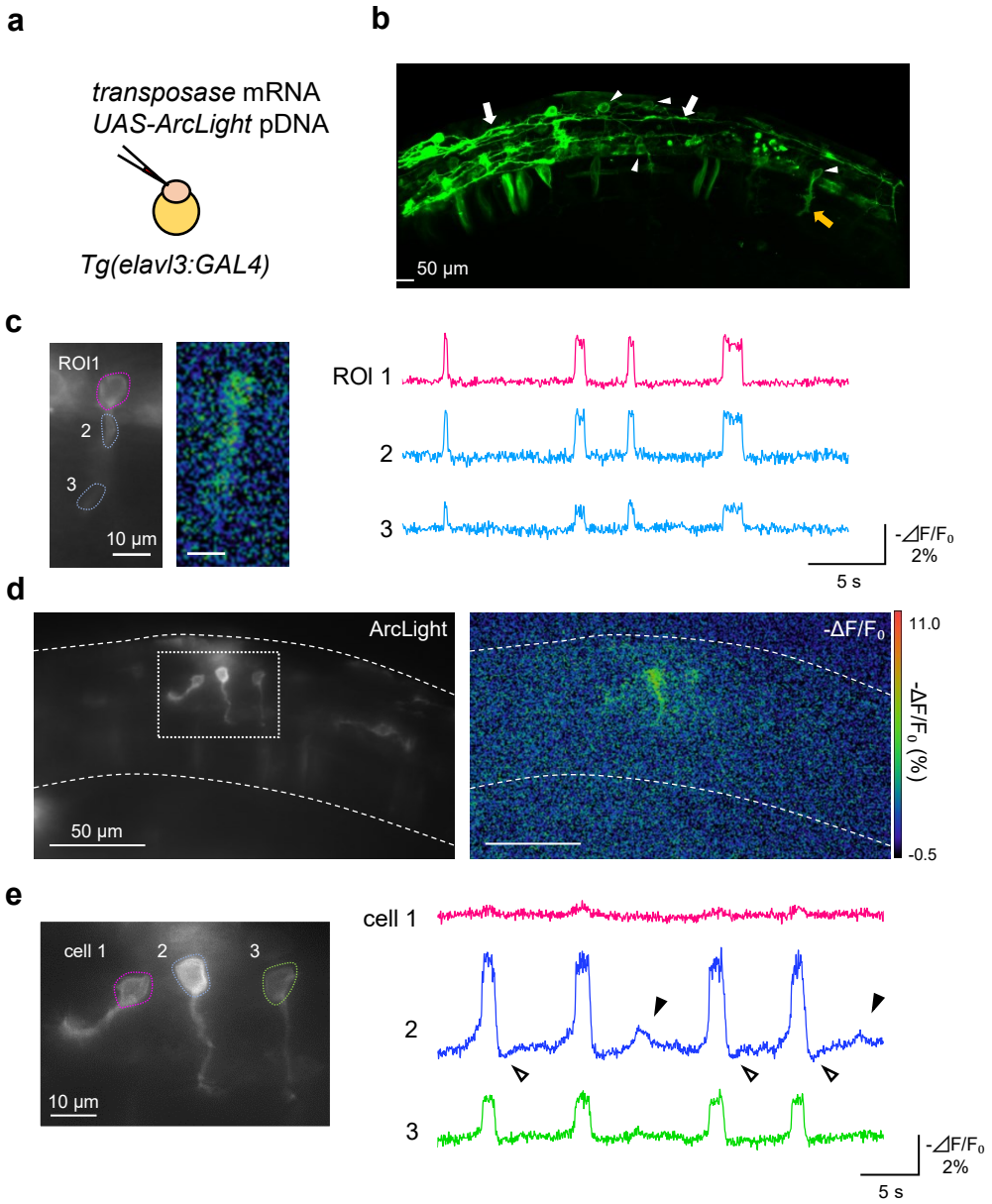
a
transposase mRNA
UAS-ArcLight pDNA
Tg(elavl3:GAL4)
b
50 μm
c
ROI1
2
3
10 μm
ROI 1
2
3
-⊿F/F0
2%
5 s
d
ArcLight
50 μm
-ΔF/F0
11.0
-ΔF/F0 (%)
-0.5
e
cell 1
2
3
10 μm
cell 1
2
3
-⊿F/F0
2%
5 s

Figure 5

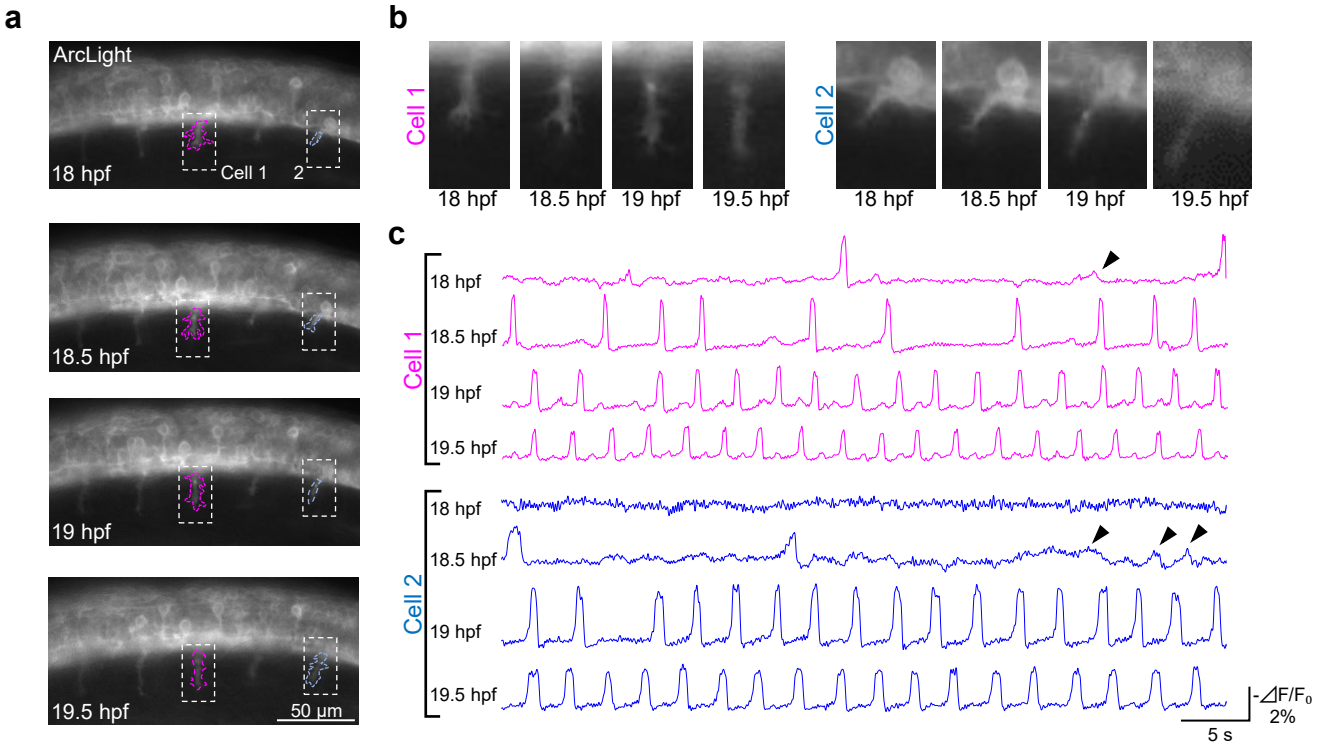
a
ArcLight
18 hpf
Cell 1
2
18.5 hpf
19 hpf
19.5 hpf
50 µm
b
Cell 1
Cell 2
18 hpf
18.5 hpf
19 hpf
19.5 hpf
c
Cell 1
Cell 2
18 hpf
18.5 hpf
19 hpf
19.5 hpf
-⊿F/F0
2%
5 s

Figure 6

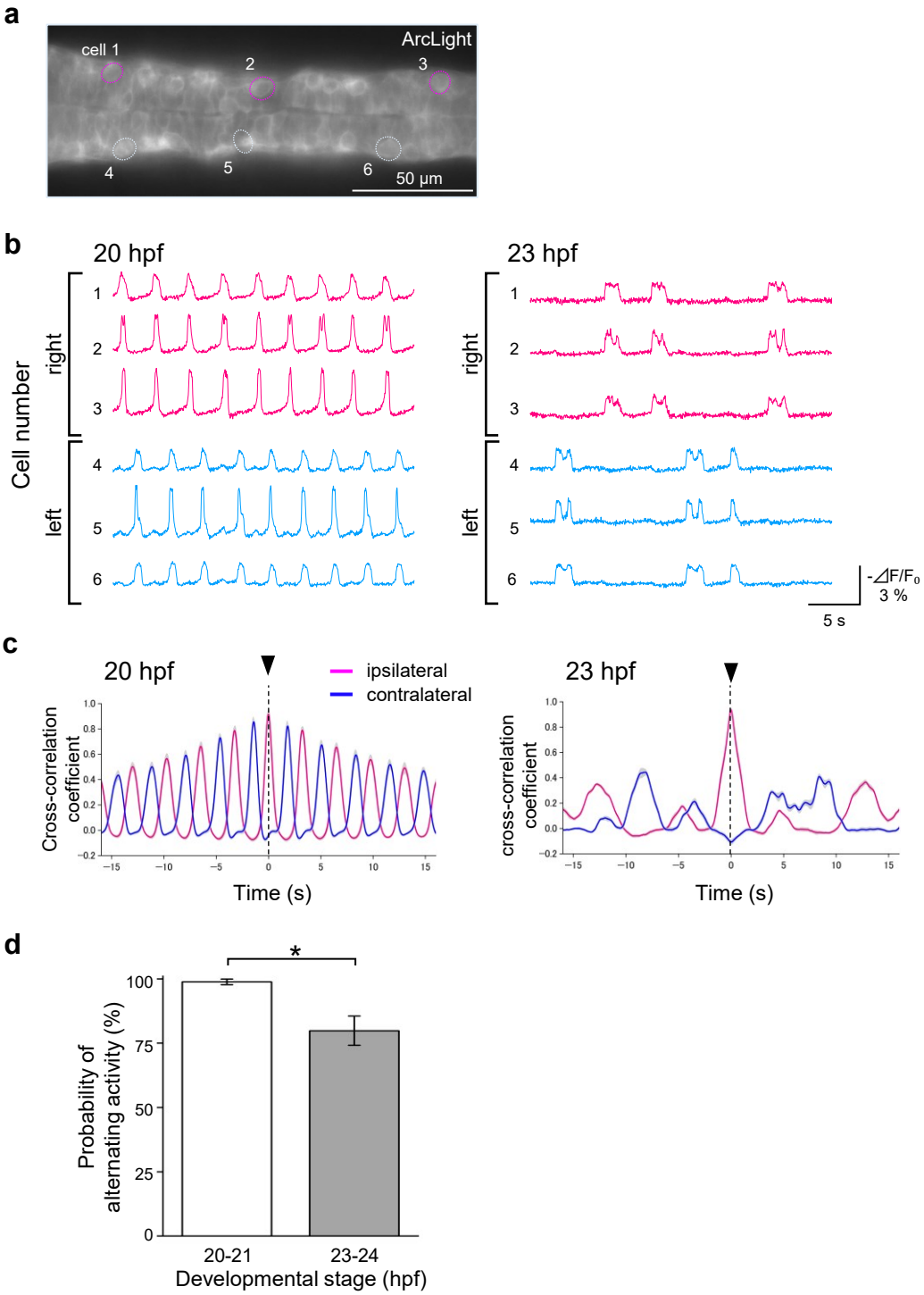
a
ArcLight
cell 1
2
3
4
5
6
50 µm
b
20 hpf
23 hpf
Cell number
right
left
1
2
3
4
5
6
-⊿F/F0
3 %
5 s
c
20 hpf
23 hpf
ipsilateral
contralateral
Cross-correlation coefficient
cross-correlation coefficient
Time (s)
d
*
Probability of alternating activity (%)
100
75
50
25
0
20-21
23-24
Developmental stage (hpf)

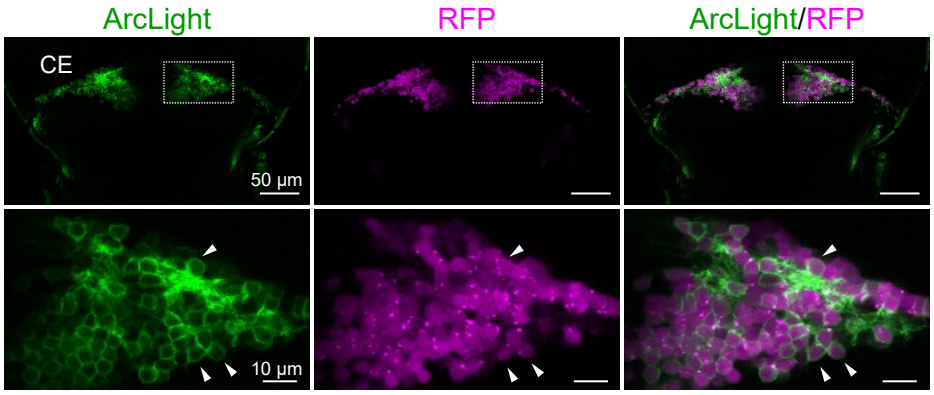

Supplementary Figure S1

a

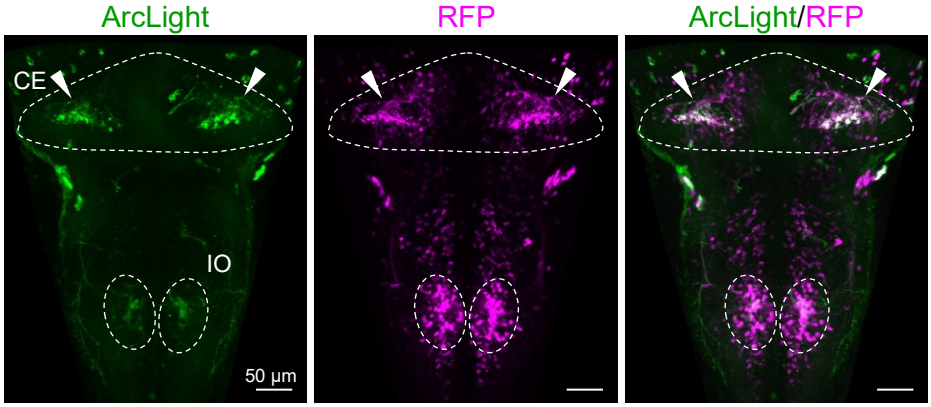

b

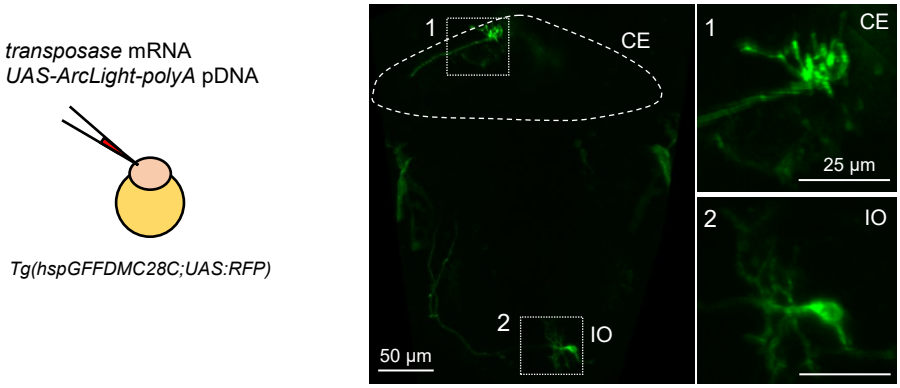

Supplementary Figure S2

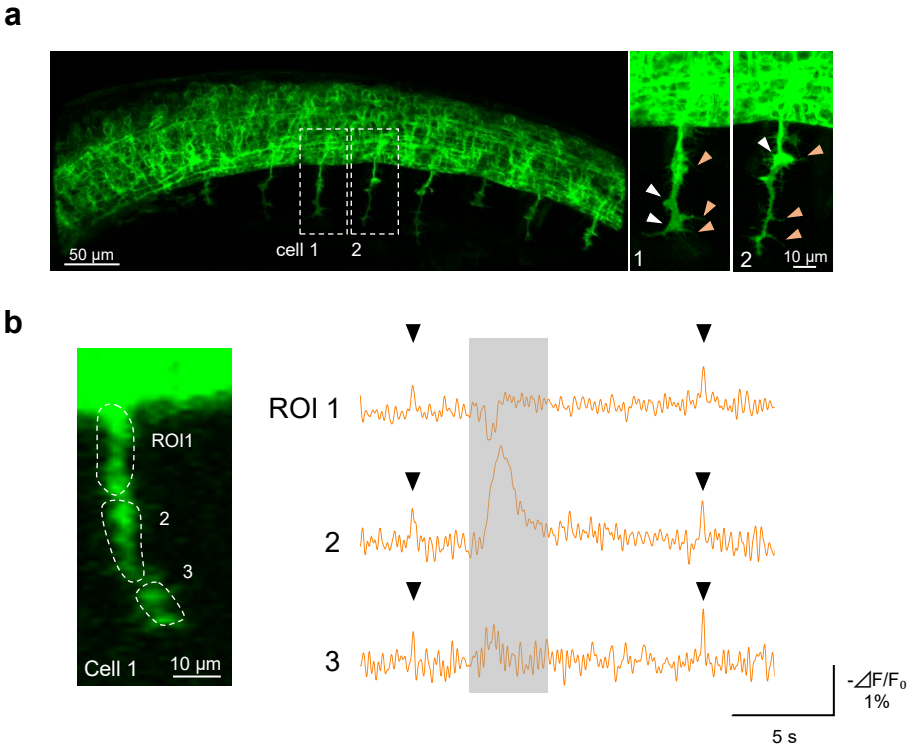

Supplementary Figure S3

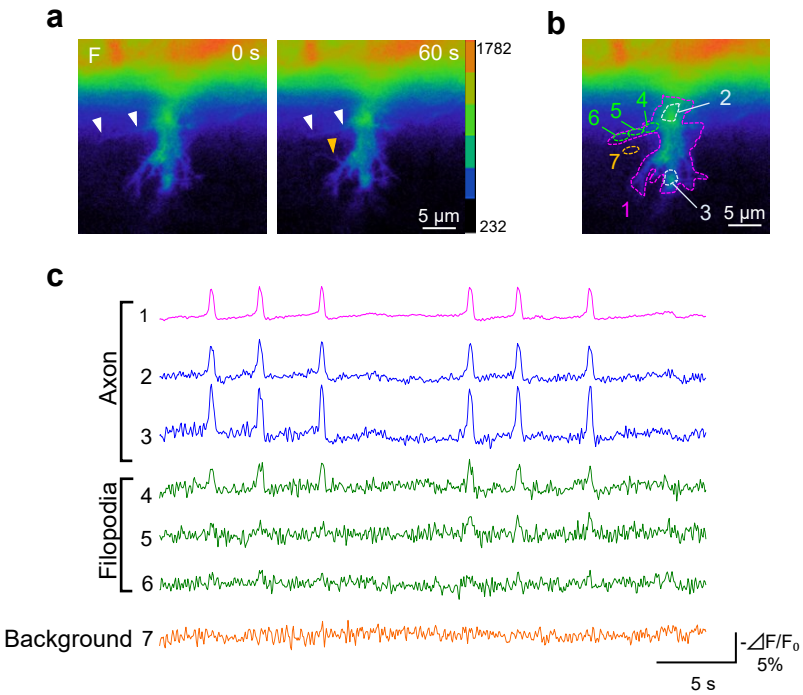

Supplementary Figure S4

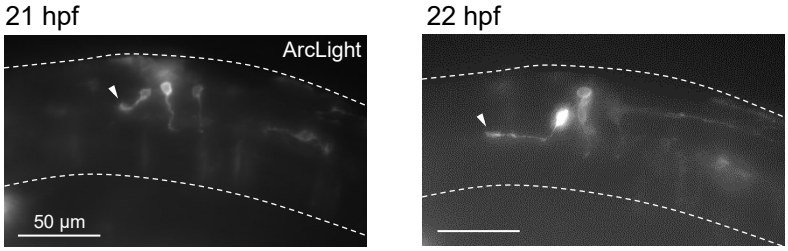

Supplementary Figure S5

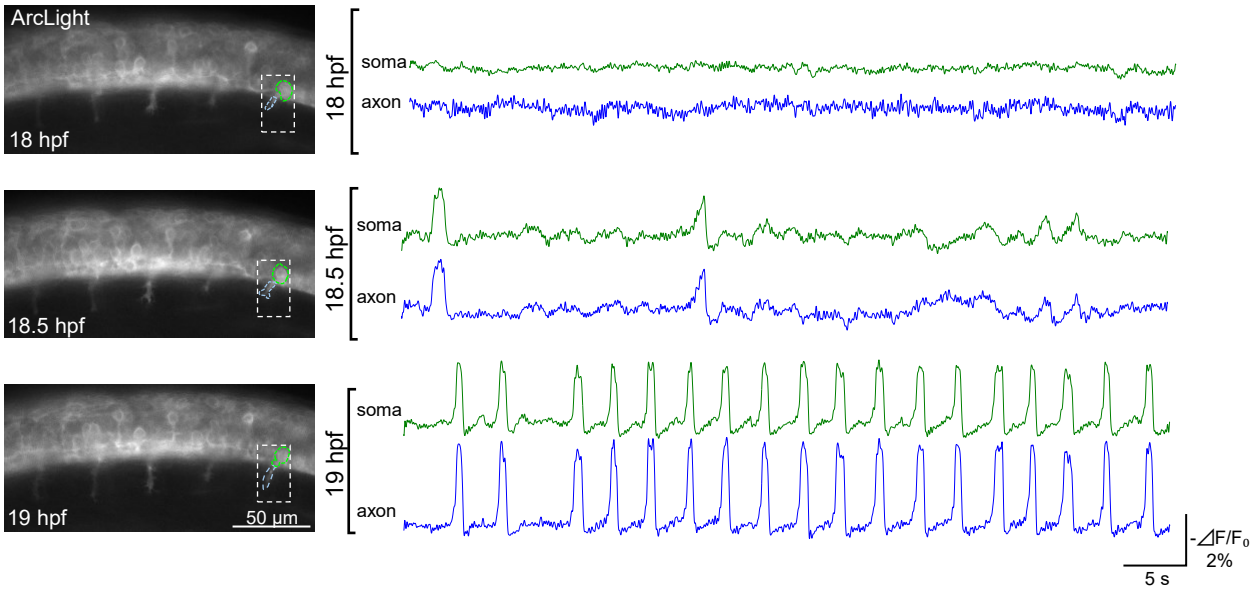

Supplementary Figure S6

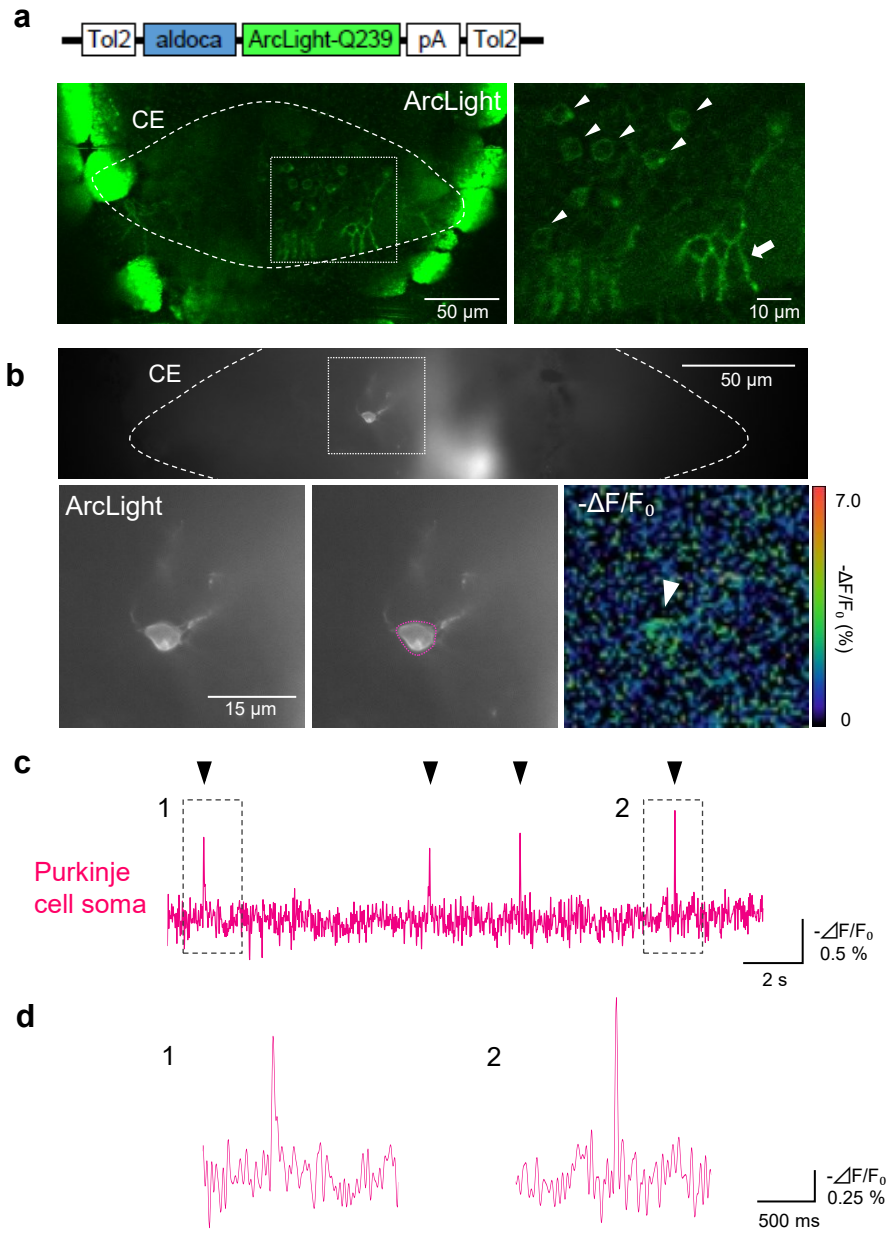

Supplementary Figure S7

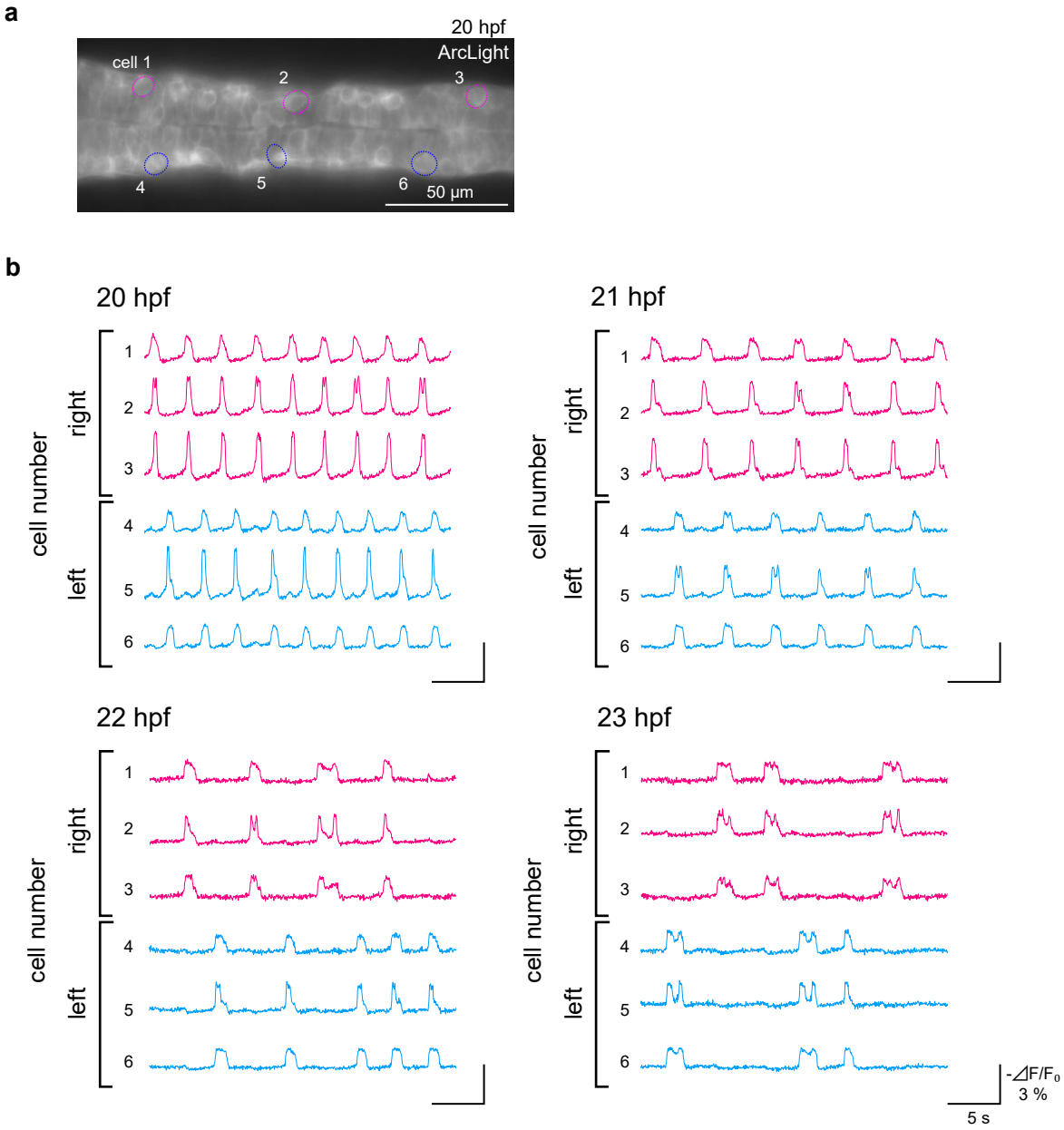

Supplementary Figure S8